

Self-similar and Universal Dynamics in Drainage of Mobile Soap Films

Antoine Monier,^{1,*} François-Xavier Gauci,¹ Cyrille Claudet,¹
 Franck Celestini,¹ Christophe Brouzet,¹ and Christophe Raufaste^{1,2}

¹*Université Côte d'Azur, CNRS, Institut de Physique de Nice (INPHYNI), 06200 Nice, France*

²*Institut Universitaire de France (IUF), 75005 Paris, France*

(Dated: January 9, 2024)

Vertical soap films drain under the influence of gravity, as indicated by the downward motion of colorful horizontal interference fringes observed on their surfaces. In this study conducted with rectangular soap films, we experimentally characterize the descent dynamics of these isothickness fringes and report its self-similar nature. We also show that this result is equivalent to thickness profiles exhibiting a separation of space and time. By integrating new measurements with data from the literature across various conditions, we validate these properties and establish the universality of the dynamics, governed by a single physical scalar. Our findings provide new insights for proposing a drainage model and understanding the mechanism of marginal regeneration at the origin of the process.

Soap films are thin liquid membranes with very particular properties. They maintain their shape at rest, like solids, forming minimal surfaces that have intrigued numerous scientists since the work of Plateau [1]. Simultaneously, their liquid nature enables soap films to be generated [2, 3] and to accommodate large deformations or self-heal when subject to perturbations [4–12]. Soap films exist across various scales, ranging from giant soap films [13, 14] to micrometer-sized soap films observed at the interfaces between bubbles within liquid foams [15]. Understanding and controlling the stability of soap films inside liquid foams is a multifactorial problem of paramount importance for industrial applications [16]. The drainage of soap films under the influence of gravity has a direct effect on their thinning dynamics and lifetime, as highlighted by the work of Mysels *et al.* [17]. The authors identified two limit cases while considering vertical soap films made from different kind of surfactant solutions. Slow drainage was observed for “rigid” films that offer high resistance to any motion within the plane of the film, in contrast to the fast drainage of “mobile” films. The latter are characterized by a smooth thickness profile associated with downward motion in the central part of the film, coupled with upward and rapid turbulent motion along the lateral borders of the film (Fig. 1(a)). This lateral flow has been identified by Mysels *et al.* [17] to be triggered by the process of marginal regeneration that consists in extracting thin film portions from the meniscus connecting the soap films with the frame [18]. These thin film elements rise by surface tension driven buoyancy [19, 20] leading to an upstream flux along the lateral borders of the film and to the downstream motion in the central part of the film by area conservation [21].

Characterizing mobile film drainage faces two major challenges. Firstly, while marginal regeneration has been extensively studied [18, 22–26], there is a lack of available data or models that account for the geometry of a vertical meniscus subject to gravity. Secondly, the literature lacks a systematic procedure to characterize the

drainage dynamics in the central part of soap films. On one hand, most studies involve measuring the evolution of thickness over time at specific positions (thinning measurements) [21, 27–29]. However, the limited number of positions, often just one, is insufficient for a full spatiotemporal characterization of the thinning dynamics. On the other hand, one study has reported measurements of the positions of isothickness lines (descent measurements) as functions of time [17], raising questions about how to reconcile the thinning and descent approaches. As a consequence, there is no consensus on how to interpret these data to extract the effect of each control parameter separately. In this letter, we present a robust procedure for obtaining a comprehensive understanding of the drainage dynamics. We show the existence of a regime where the descent dynamics is self-similar and the shape of the thickness profile remains identical. For each experiment, we demonstrate that the full spatiotemporal dynamics can be described using a single parameter quantifying the typical drainage speed or thinning rate, along with a single function that characterizes the fine details of the process. By compiling data from existing literature along with new experiments, we demonstrate that this regime prevails in diverse experimental conditions, and that the function is universal in all situations encountered for mobile soap films, thus reconciling various empirical laws found in the literature.

Experiments involve creating soap films within vertical rectangular frames with varying widths W and heights H , ranging from 4 to 20 mm and from 5 to 30 mm, respectively. These frames are constructed from glass fibers with a diameter of 700 μm , meticulously joined edge to edge. The surfactant solutions were comprised of water-glycerol mixtures, with sodium dodecyl sulfate (SDS) present at a concentration of 5.6 g.L^{-1} . We systematically adjusted the water-glycerol ratio to modulate the bulk viscosity η within the range of 1 to 20 mPa.s . The surface tension γ is estimated at 32 mN.m^{-1} [30].

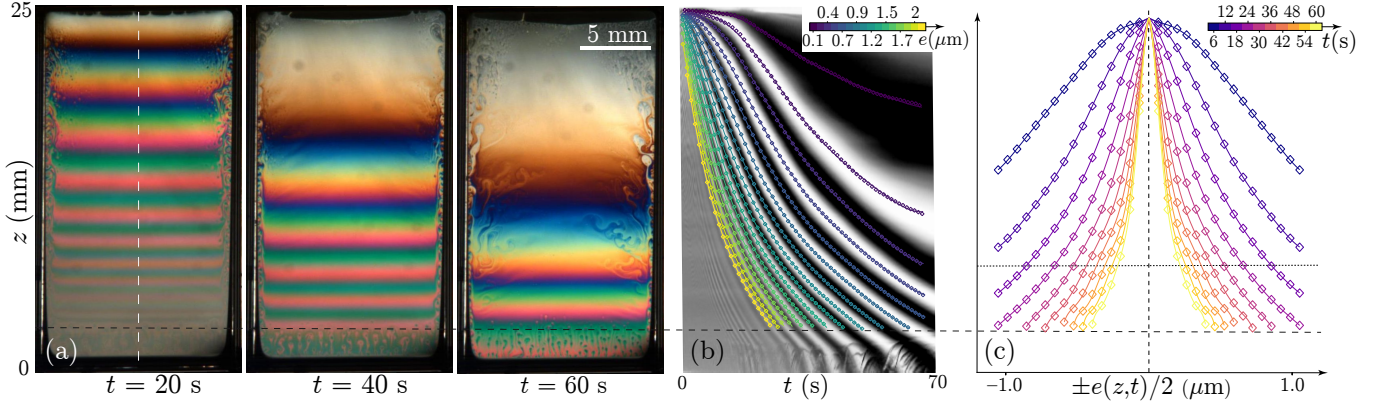


FIG. 1. (a) Temporal snapshots of an experiment: $W = 16$ mm, $H = 25$ mm, $\eta = 1.5$ mPa.s. The central part shows horizontal interference fringes of homogeneous thickness. Marginal regeneration is observed at the lateral and bottom borders (below dashed line). (b) Spatiotemporal diagram obtained along the white dashed line in (a). Colour-coded iso-thickness centers are tracked and lines interpolate points. (c) Thickness profile at different times, in colors. The dotted line indicates $z^*/H = 0.3$.

In each experiment, the frame was fully immersed in the surfactant solution and then swiftly removed, typically within 1 second. The position inside the film is identified by the coordinate z , ranging between 0 at the bottom and H at the top. We characterized the thickness profile in the central part of the soap film using thin-film interferences, coding for the local thickness of the film [31]. White light is reflected at the film's surface, and the evolving interference patterns were recorded with a color camera. To minimize the impact of evaporation [32], the entire setup was placed inside a controlled humidity chamber with high relative humidity, typically at $H_r \geq 85\%$. Depending on the parameters, it takes between 20 s and 30 min for the $0.2 \mu\text{m}$ -thick fringe to reach $z/H = 0.5$.

Fig. 1(a) displays three snapshots of a typical experiment, illustrating the temporal evolution of the interference pattern. Each colored fringe, representing an isothickness line, moves downward, thus indicating a global thinning process. In the region of interest, there is nearly no black film at the top, allowing us to assume that the thickness gradually approaches zero at $z = H$. Similarly, at the bottom of the film, a small region (below the black dashed line in Fig. 1) is disrupted by thin elements, originating from marginal regeneration. It is worth noting that this process at the bottom of the film is expected to have a negligible impact on thinning dynamics, unlike marginal regeneration at the lateral borders. Apart from these edge effects, the pattern remains smooth, confirming a regular thickness profile from top to bottom in the central part of the film. We initially performed descent measurements that involved tracking the center positions of isothickness lines corresponding to intensity maxima and minima while using 660 nm filtered light (spatiotemporal diagram in Fig. 1(b)). In an experiment, roughly fifteen fringes are tracked corresponding to thicknesses

ranging between 0.1 and $2 \mu\text{m}$. For a given film thickness e , we denoted $z(e, t)$ the position of this thickness with respect to time. We noticed that the larger e , the faster the process and the time evolution of $z(e, t)$. Then, thinning measurements were deduced from the same set of data and thickness profiles $e(z, t)$ were calculated for different times as displayed in Fig. 1(c).

In Fig. 1(b), we observe that all curves display the same behavior whatever e within one time dilation factor: the evolution of z for a given e starts slowly, accelerates, and then slows down at a later stage. This evolution marks the presence of an inflection point, highlighting a maximum in speed that occurs at a fixed position $z_{\text{max}} \simeq 0.8H$, regardless of the thickness (see Supplemental Material [33]). These elements suggest that the descent dynamics exhibits self-similarity such as

$$z(e, t) = H f \left(\frac{t - t_0}{T(e)} \right), \quad (1)$$

with f a function varying between 0 and 1, $T(e)$ a function of e that quantifies scale invariance in time, and t_0 a fit parameter that marks the onset of this regime. This self-similarity is confirmed by collapsing all isothickness positions of experiment in Fig. 1(b) onto the same master curve in Fig. 2(a), with the arbitrary constraint $f(1) = 0.8$, and a procedure to measure t_0 detailed in Supplemental Material [33]. This leads to a very good collapse and the determination of $T(e)$, which exhibits an e^{-1} dependency as shown in the inset of Fig. 2(a). Consequently, we define

$$T(e) = \frac{\kappa}{e}, \quad (2)$$

where κ is constant for a given experiment and is expected to reflect the influence of control parameters on the time evolution of the isothickness lines' positions. To

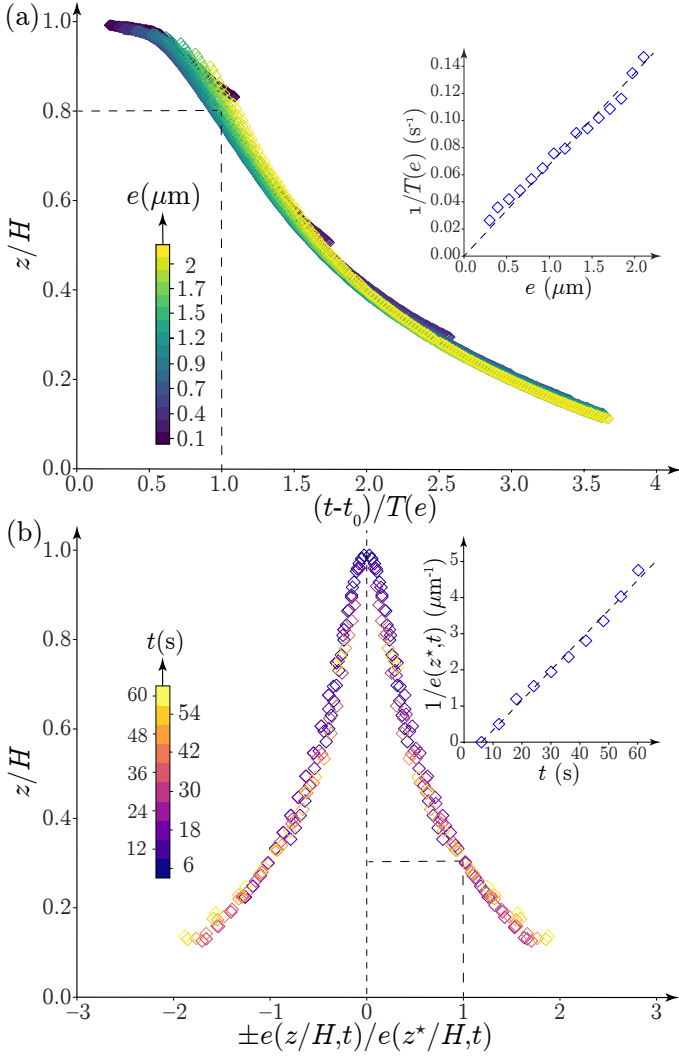


FIG. 2. (a) Rescaled descent positions from Fig. 1(b) with color coding for thickness. Inset shows the proportionality between the scaling time $1/T(e)$ and e . (b) Rescaled thickness profiles from Fig. 1(c) with color coding for time. Inset shows the affine behavior of $1/e(z^*/H,t)$ as a function of time.

conclude, for a given experiment, the descent dynamics exhibits a self-similar process fully described by two quantities: a physical scalar κ with units of m.s and a dimensionless function f .

Given that $T(e) \propto e^{-1}$, it is possible to switch from the descent approach to the thinning approach, additionally revealing a separation of space and time variables in the latter. In fact, Eqs. (1) and (2) result in

$$e(z,t) = \frac{\kappa}{t-t_0} f^{-1} \left(\frac{z}{H} \right). \quad (3)$$

This equation predicts a thickness evolution in $\kappa/(t-t_0)$ for a given position in space: if we note z^* a fixed position

between 0 and H ,

$$e(z^*,t) \propto \frac{\kappa}{t-t_0}, \quad (4)$$

and Eq.(3) can thus be expressed as

$$e(z,t) = e(z^*,t) S_{z^*} \left(\frac{z}{H} \right), \quad (5)$$

where S_{z^*} is a shape function that is proportional to f^{-1} with a constant that depends on the chosen measurement position z^* to ensure $S_{z^*} \left(\frac{z}{H} \right) = 1$ in $z = z^*$. The predictions of Eqs. (4) and (5) are tested with the same dataset used in Fig. 1. In Fig. 2(b), we observe that all thickness profiles at successive times collapse onto a single curve when plotting $e(z,t)/e(z^*,t)$ as a function of z/H , with $z^* = 0.3 H$ marked by the dashed line in Fig. 1(c). The time evolution of $e(z^*,t)$ is consistent with Eq. (4), as evidenced by the affine behavior when plotting $1/e(z^*,t)$ as function of t (inset of Fig. 2(b)). To conclude, for a given experiment, the thinning dynamics is characterized by a unique thickness profile, up to a multiplicative factor that decreases inversely proportional to time.

We systematically studied the validity of our approach by varying the frame dimensions, including width W and height H , as well as the bulk viscosity η of the solution. 18 different experimental conditions were tested (see Supplemental Material [33]) with typically a factor 90 between the slowest and fastest dynamics. In the descent approach, the function f describes the time evolution of the positions of isothickness lines up to multiplicative scaling factors (Eq. (1)). In Fig. 3(a), the function f is plotted for several values of the parameters W , H and η . Very remarkably, all experiments aggregate onto the same curve, suggesting the function f to be universal for this set of parameters. In particular, the inflection point, which indicates the presence of a maximum speed, is consistently located at $0.8 H$ for all values of e whatever the experimental conditions. The same holds for the thinning approach. As defined previously, f is intrinsically linked to the shape functions S_{z^*} as $S_{z^*} \propto f^{-1}$ for any z^* between 0 and H . The universality of the function S_{z^*} with $z^* = 0.3 H$ is demonstrated in the right-hand side of Fig. 3(b) using the same dataset. Our findings consistently show that regardless of the parameters employed and time scales at play, the function f remains universal.

Furthermore, this assertion is tested using available data from the literature that provide thickness profile measurements at different times under various experimental conditions [17, 27, 34, 35]. S_{z^*} with $z^* = 0.3 H$ obtained from these profiles is displayed on the left-hand side of Fig. 3(b) for comparison with our data shown on the right-hand side of the same figure. In all cases, S_{z^*} is remarkably similar for $z/H > 0.2$. For $z/H < 0.2$

(grey zone in Fig. 3(b)), the profiles no longer superimpose, a fact that we attribute to the presence of thin film elements generated at the bottom border by marginal regeneration, perturbing the thickness profiles.

Another validation of our prediction is that $e(z^*, t)$ evolves inversely proportional to time, as expected from Eq. (4), for the same datasets taken from the literature (see Supplemental Material [33]), confirming the results obtained with our experimental setup. This time dependence is also validated with studies providing measurements of the thickness at a given position only [21, 27–29]. Hudales *et al.* [27] found that the local thinning rate, $\partial e / \partial t$, scales as $-e^2$, which is fully consistent with a law $e(z^*, t) \propto 1/(t - t_0)$. Berg *et al.* [28] characterized the evolution of the thickness with an empirical law that is simplified in the long time limit as $(t - t_0)^\beta$, with measured exponents β around -1. This exponent is retrieved in Tan *et al.* [29], and we have verified that the same value can be inferred from the data of Seiwert *et al.* [21]. All these data support the assertion of a universal function f and a local thickness that evolves inversely proportional to time in numerous experimental conditions.

In conclusion, our study demonstrates that the drainage of mobile soap films can be characterized using either of two approaches. In the descent approach, the positions of isothickness lines exhibit self-similarity with a scaling time inversely proportional to the film thickness, whereas in the thinning approach, the shape of the thickness profiles remains identical in space but evolves as $(t - t_0)^{-1}$ in time. In both approaches, the dynamics is characterized by two quantities only: a physical scalar κ and a dimensionless function f . To maintain consistency, t_0 should also be considered, but its significance is secondary. It marks the onset of the regime of interest, which, in practice, is roughly equivalent to the time the frame is removed from the surfactant solution. The exact value of t_0 might be associated with the transient period between film formation, where the thickness corresponds to the value expected from Frankel’s law, and the initiation of the thinning process [28].

Our analysis suggests that f is a universal function. This highlights that the mechanisms at play are the same, and only the time or speed scales differ between different setups or experimental conditions. However, certain conditions must be met for this regime to be observed. For instance, it is essential to neglect the effects of evaporation to obtain the f function depicted in Fig. 3. Additionally, edge effects at both the top and bottom should be minimized. On the top, the extent of the black film should remain small, which is not always the case with certain surfactants or over extended drainage periods [36]. The region affected by thin film elements generated at the bottom edge should also be of limited spatial extent. These considerations support our choice of fix-

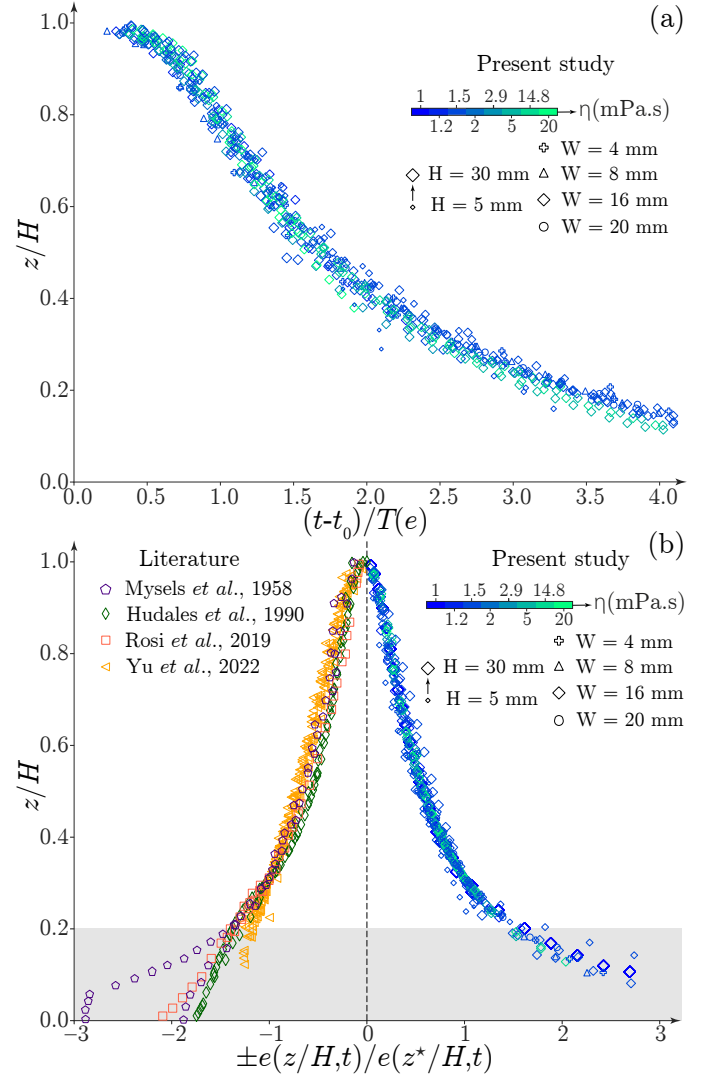


FIG. 3. (a) Rescaled descent positions for all experiments. Marker types represent widths, marker sizes correspond to heights, and marker colors indicate viscosity. For clarity, only two isothickness lines are plotted for each experiment—one with a small thickness and one with a large thickness. 36 isothickness lines are displayed out of a set of 300 available. (b) Rescaled thickness profiles: the right side displays our data with the same markers as in (a), while the left side shows data from the literature. Again, only two temporal profiles are retained for each experiment. The grey zone highlights the values $z < 0.2H$ that often correspond to the presence of marginal regeneration at the bottom border of the soap film.

ing $z^* = 0.3H$ as a suitable compromise, as this value is small enough to provide a good signal-to-noise ratio but not so small that it avoids the region perturbed by the rising thin film elements.

κ is the scalar of primary interest. Our study reveals that drainage can be characterized either by a typical time scaling proportional to κ/e or by a typical descent speed scaling as He/κ . Notably, our study identifies, for the first time, a scaling with respect to e , which is

absent in existing models in the literature [17, 18, 21]. This suggests the need for model improvements to gain a better understanding of how marginal regeneration and the upward flow along the lateral borders, whose effect is evidenced by the scaling $\kappa \propto W$ (References [17, 21, 27, 28] and Supplemental Material [33] for the present study), impact the overall dynamics. To address this, additional experimental data are needed to discern the influence of the other control parameters on κ .

This work was supported by the National Research Agency (ANR-20-CE30-0019). The authors are grateful to Emma Simon for her participation at the early stage of the project, and to Isabelle Cantat and Emmanuelle Rio for fruitful discussions.

* antoine.monier@univ-cotedazur.fr

- [1] J. Plateau, *Statique expérimentale et théorique des liquides soumis aux seules forces moléculaires* (Gauthier-Villars, Paris, France, 1873).
- [2] E. a. V. Nierop, B. Scheid, and H. A. Stone, On the thickness of soap films: an alternative to Frankel's law, *Journal of Fluid Mechanics* **602**, 119 (2008).
- [3] L. Saulnier, F. Restagno, J. Delacotte, D. Langevin, and E. Rio, What Is the Mechanism of Soap Film Entrainment?, *Langmuir* **27**, 13406 (2011).
- [4] Y.-J. Chen and P. H. Steen, Dynamics of inviscid capillary breakup: collapse and pinchoff of a film bridge, *Journal of Fluid Mechanics* **341**, 245 (1997).
- [5] L. Courbin and H. A. Stone, Impact, puncturing, and the self-healing of soap films, *Physics of Fluids* **18**, 091105 (2006).
- [6] T. Gilet and J. W. M. Bush, The fluid trampoline: droplets bouncing on a soap film, *Journal of Fluid Mechanics* **625**, 167 (2009).
- [7] R. E. Goldstein, H. K. Moffatt, A. I. Pesci, and R. L. Ricca, Soap-film Möbius strip changes topology with a twist singularity, *PNAS* **107**, 21979 (2010).
- [8] G. Kirstetter, C. Raufaste, and F. Celestini, Jet impact on a soap film, *Phys. Rev. E* **86**, 036303 (2012).
- [9] R. E. Goldstein, J. McTavish, H. K. Moffatt, and A. I. Pesci, Boundary singularities produced by the motion of soap films, *PNAS* **111**, 8339 (2014).
- [10] L. Salkin, A. Schmit, P. Panizza, and L. Courbin, Generating Soap Bubbles by Blowing on Soap Films, *Phys. Rev. Lett.* **116**, 077801 (2016).
- [11] B. B. Stogin, L. Gockowski, H. Feldstein, H. Claire, J. Wang, and T.-S. Wong, Free-standing liquid membranes as unusual particle separators, *Science Advances* **4**, eaat3276 (2018).
- [12] R. E. Goldstein, A. I. Pesci, C. Raufaste, and J. D. Shemilt, Geometry of catenoidal soap film collapse induced by boundary deformation, *Phys. Rev. E* **104**, 035105 (2021).
- [13] P. Ballet and F. Graner, Giant soap curtains for public presentations, *Eur. J. Phys.* **27**, 951 (2006).
- [14] S. Mariot, M. Pasquet, V. Klein, F. Restagno, and E. Rio, A new setup for giant soap films characterization, *The European Physical Journal E* **44**, 1 (2021).
- [15] I. Cantat, S. Cohen-Addad, F. Elias, F. Graner, R. Höhler, O. Pitois, F. Rouyer, and A. Saint-Jalmes, *Foams: structure and dynamics* (OUP Oxford, 2013).
- [16] P. Stevenson, Foam Engineering, in *Foam Engineering* (John Wiley & Sons, Ltd, 2012).
- [17] K. J. Mysels, S. Frankel, and K. Shinoda, *Soap films: studies of their thinning and a bibliography* (Pergamon press, 1959).
- [18] A. Gros, A. Bussonnière, S. Nath, and I. Cantat, Marginal regeneration in a horizontal film: Instability growth law in the nonlinear regime, *Phys. Rev. Fluids* **6**, 024004 (2021).
- [19] Y. Couder, J. Chomaz, and M. Rabaud, On the hydrodynamics of soap films, *Physica D: Nonlinear Phenomena* **37**, 384 (1989).
- [20] N. Adami and H. Caps, Capillary-driven two-dimensional buoyancy in vertical soap films, *EPL (Europhysics Letters)* **106**, 46001 (2014).
- [21] J. Seiwert, R. Kervil, S. Nou, and I. Cantat, Velocity field in a vertical foam film, *Physical Review Letters* **118**, 048001 (2017).
- [22] A. Aradian, E. Raphael, and P.-G. De Gennes, "marginal pinching" in soap films, *EPL (Europhysics Letters)* **55**, 834 (2001).
- [23] V. A. Nierstrasz and G. Frens, Marginal regeneration in thin vertical liquid films, *Journal of colloid and interface science* **207**, 209 (1998).
- [24] H. Lhuissier and E. Villermaux, Bursting bubble aerosols, *Journal of Fluid Mechanics* **696**, 5 (2012).
- [25] J. Miguet, M. Pasquet, F. Rouyer, Y. Fang, and E. Rio, Marginal regeneration-induced drainage of surface bubbles, *Physical Review Fluids* **6**, L101601 (2021).
- [26] C. Tréguët and I. Cantat, Instability of the one-dimensional thickness profile at the edge of a horizontal foam film and its plateau border, *Physical Review Fluids* **6**, 114005 (2021).
- [27] J. Hudaes and H. Stein, Marginal regeneration of a mobile vertical free liquid film, *Journal of colloid and interface science* **138**, 354 (1990).
- [28] S. Berg, E. A. Adelizzi, and S. M. Troian, Experimental study of entrainment and drainage flows in microscale soap films, *Langmuir* **21**, 3867 (2005).
- [29] S. N. Tan, Y. Yang, and R. G. Horn, Thinning of a vertical free-draining aqueous film incorporating colloidal particles, *Langmuir* **26**, 63 (2010).
- [30] A. Bussonnière, E. Shabalina, X. Ah-Thon, M. Le Fur, and I. Cantat, Dynamical coupling between connected foam films: Interface transfer across the menisci, *Physical Review Letters* **124**, 018001 (2020).
- [31] L. J. Atkins and R. C. Elliott, Investigating thin film interference with a digital camera, *American Journal of Physics* **78**, 1248 (2010).
- [32] L. Champougny, J. Miguet, R. Henaff, F. Restagno, F. Boulogne, and E. Rio, Influence of evaporation on soap film rupture, *Langmuir* **34**, 3221 (2018).
- [33] See Supplemental Material at [URL will be inserted by the publisher] for movies, details about experimental conditions, characterization of the descent dynamics, κ measurements, and rescaling of the thickness profiles from literature data.
- [34] T. Rosi, L. M. Gratton, P. Onorato, and S. Oss, Light interference from a soap film: a revisited quasi-monochromatic experiment, *Physics Education* **54**,

- [015018 \(2019\)](#).
- [35] X. Yu, K. Qiu, X. Yu, Q. Li, R. Zong, and S. Lu, Stability and thinning behaviour of aqueous foam films containing fluorocarbon and hydrocarbon surfactant mixtures, [Journal of Molecular Liquids](#) **359**, 119225 (2022).
- [36] S. Sett, S. Sinha-Ray, and A. Yarin, Gravitational drainage of foam films, [Langmuir](#) **29**, 4934 (2013).

SUPPLEMENTAL MATERIAL

Movies

Movie “Movie1.avi” features the video used in Fig. 1 under the experimental conditions: $W = 16$ mm, $H = 25$ mm, $\eta = 1.5$ mPa.s, accelerated three times.

Movie “Movie2.avi” displays four soap films with different widths $W = [4, 8, 16, 20]$ mm (the soap film with a 20 mm width is truncated in the video), under the same conditions as in movie “Movie1.avi”, accelerated three times. In this movie, time is stopped independently for each soap film when the same fringe reaches the same position. This illustrates that the same thickness profile is obtained for different times, highlighting universality in the shape of the thickness profile.

Movie “Movie3.avi” presents the temporal animated plot of Fig. 1(c) for every time step. The video is accelerated three times, and colors represent time.

Experimental conditions

While the SDS concentration is fixed at 5.6 g.L^{-1} in experiments, we tested 18 different experimental conditions by varying frame width W , frame height H , and viscosity η of the solution, as shown in Tab. I.

Width W (mm)	Height H (mm)	Viscosity η (mPa.s)
4	25	1.5
8	25	1.5
16	25	1.5
20	25	1.5
16	25	1
16	25	1.2
16	25	2
16	25	2.9
16	25	5
16	25	14.8
16	25	20
16	5	1.5
16	7.5	1.5
16	10	1.5
16	12.5	1.5
16	15	1.5
16	20	1.5
16	30	1.5

TABLE I. Experimental conditions.

Self-similar descent dynamics - determination of t_0

For each experiment and regardless of e , the time evolution of $z(e, t)$ starts slowly, accelerates, and then slows down at a later stage. Consequently, the time evolution of the speed for a given e , $V(e, t) = |\partial z / \partial t|$, exhibits a

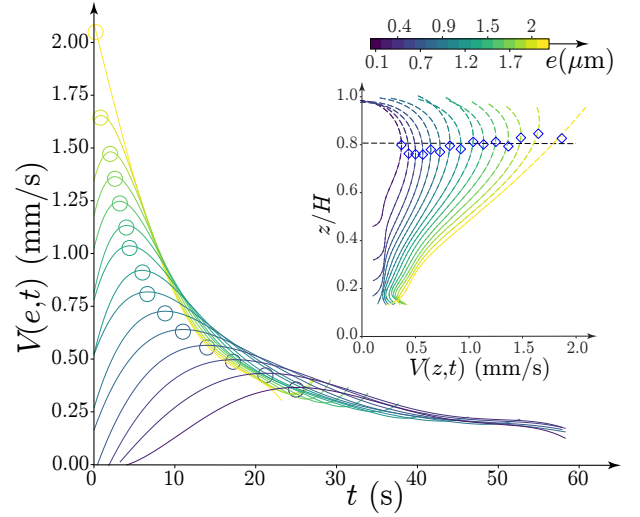


FIG. 4. Descent speed as a function of time for various thicknesses, indicated by different colors. The positions of the maximum speeds are marked with open circles. This maximum is observed at a position $z_{\max} \simeq 0.8 H$, which does not depend on the fringe thickness e , as shown by the inset.

maximum $V_{\max}(e)$ at a time $t_{\max}(e)$ (Fig. 4), and the larger e , the larger $V_{\max}(e)$ and the smaller $t_{\max}(e)$. Remarkably, $V_{\max}(e)$ always occurs at a fixed position $z_{\max}(e) \simeq 0.8 H$ regardless of e (inset of Fig. 4).

In what follows, we show the existence of a relationship between V_{\max} and t_{\max} that supports the hypothesis of self-similarity given by the equation $z(e, t) = H f\left(\frac{t-t_0}{T(e)}\right)$. Taking the time derivative of this equation gives:

$$\dot{z}(e, t) = \frac{H}{T(e)} f' \left(\frac{t-t_0}{T(e)} \right).$$

At $t = t_{\max}(e)$, the speed is maximum. Given that isotherm lines are moving downward, f' is negative, and the maximum speed is written as

$$V_{\max}(e) = \frac{H}{T(e)} \left| f' \left(\frac{t_{\max}(e) - t_0}{T(e)} \right) \right|$$

If we define $u = \frac{t-t_0}{T(e)}$ and $u_{\max} = \frac{t_{\max}(e) - t_0}{T(e)}$, we can identify an affine relationship between t_{\max} and $1/V_{\max}$,

$$t_{\max}(e) = C \frac{1}{V_{\max}(e)} + t_0,$$

with $C = H u_{\max} |f'(u_{\max})|$ as the slope and t_0 as the intercept. This relation is validated in Fig. 5(a), and a linear fit allows us to define C and t_0 for an experiment.

In addition, the slope C is predicted to depend proportionally on H and to be independent of other parameters such as the width W or the viscosity η . This prediction is

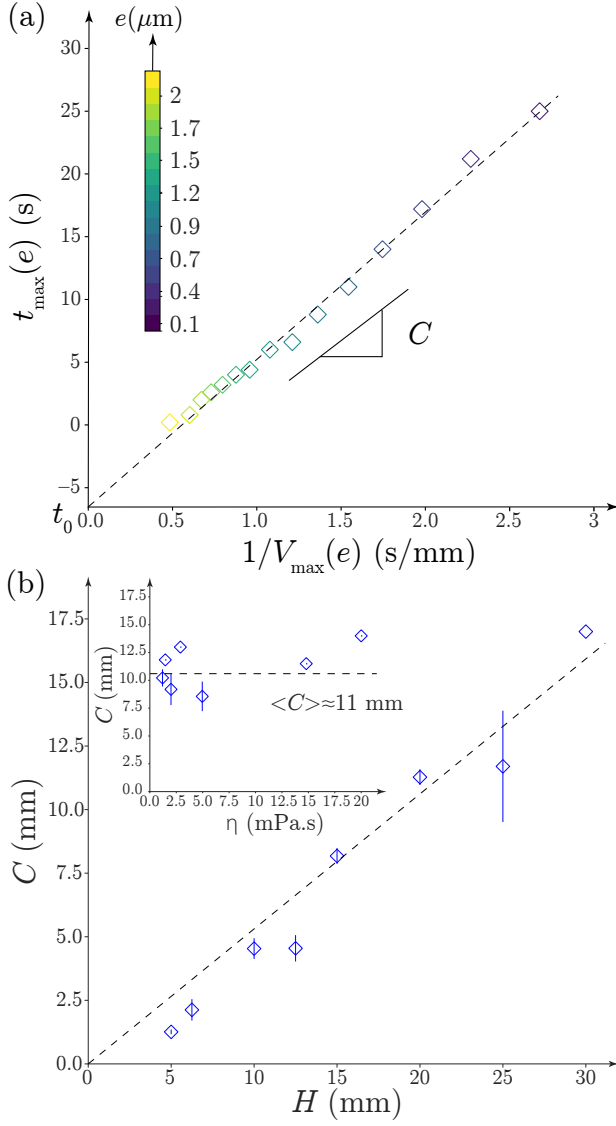


FIG. 5. (a) $t_{\max}(e)$ as a function of $1/V_{\max}(e)$. The dashed line is a fit with an affine function, and its intercept defines t_0 . (b) Self-similar coefficient C as a function of film height H . The dashed line is a fit highlighting the proportionality between the two quantities. Inset: C as a function of η for $H = 25$ mm. The dashed line is fit with a constant.

tested and validated in Fig. 5(b), showing the proportionality between C and H (main plot) and the independence between C and η as an example (inset).

κ measurements

In the thinning approach, we expect $e(z^*, t) \propto \frac{\kappa}{t-t_0}$ with a proportionality constant that depends on the choice of z^*/H . We thus define the constant κ^* , which depends on the choice of z^*/H , as $e(z^*, t) = \frac{\kappa^*}{t-t_0}$ to eval-

uate the trend of κ in thinning measurements.

Similar to κ , the scalar κ^* encapsulates the effect of the controlled parameters, such as width, height, viscosity, etc. Previous studies have already highlighted the effect of the film width on the dynamics, with a typical drainage time scale that is proportional to the width [17, 21, 27, 28]. We have verified that this result is also confirmed with our data. In the inset of Fig. 6, κ^* is extracted from thinning measurements obtained with four frames of different widths, $W = [4, 8, 16, 20]$ mm. κ^* is then plotted as a function of W , and a proportionality relation is observed (Fig. 6).

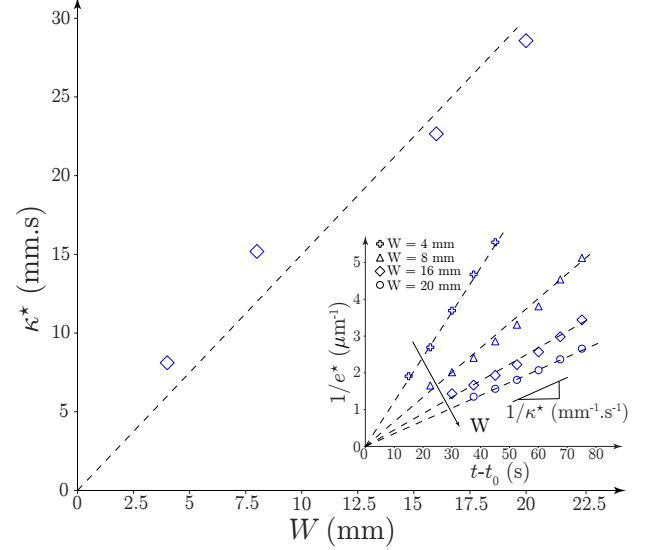


FIG. 6. κ^* as a function of W for $z^* = 0.3H$. The dashed line serves as a guide for the eye, showing the proportionality between the two quantities. Inset: $1/e^*$ as a function of $t-t_0$ for four different widths (see movie “Movie2.avi”). Dashed lines are fitted with a proportionality relation, and the slope provides $1/\kappa^*$.

Rescaling the thickness profiles from literature data.

We present here the rescaling of experimental data from the literature. For a given experiment, we first display the original thickness profiles obtained at different times. Then, we set $z^* = 0.3H$ and plot the rescaled profiles $e(z, t)/e(z^*, t)$ on one hand, and we verify the linear relationship between $1/e^*$ and t on the other hand. Fig. 7 is obtained from Hudaes *et al.* [27]. Figs. 8 and 9 are obtained from Yu *et al.* [35]: each figure corresponds to a specific surfactant solution, either comprising several SDS concentrations without FC1157, or the same SDS concentration but different FC1157 concentrations.

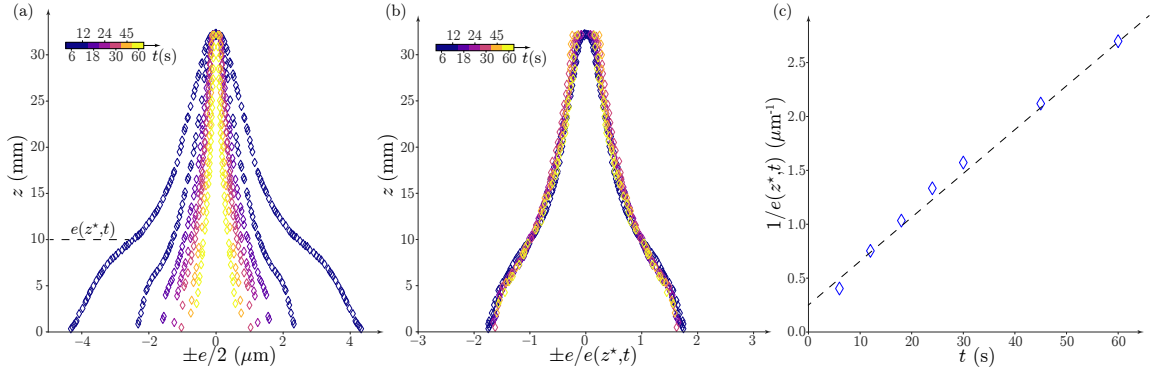


FIG. 7. (a) Thickness profiles at different times, coded in colors, adapted from Fig. 1 in Hudales *et al.* [27]. (b) Rescaled profiles obtained after normalizing by $e(z^*, t)$. (c) $1/e(z^*, t)$ as a function of t to validate the linear relationship between these two quantities.

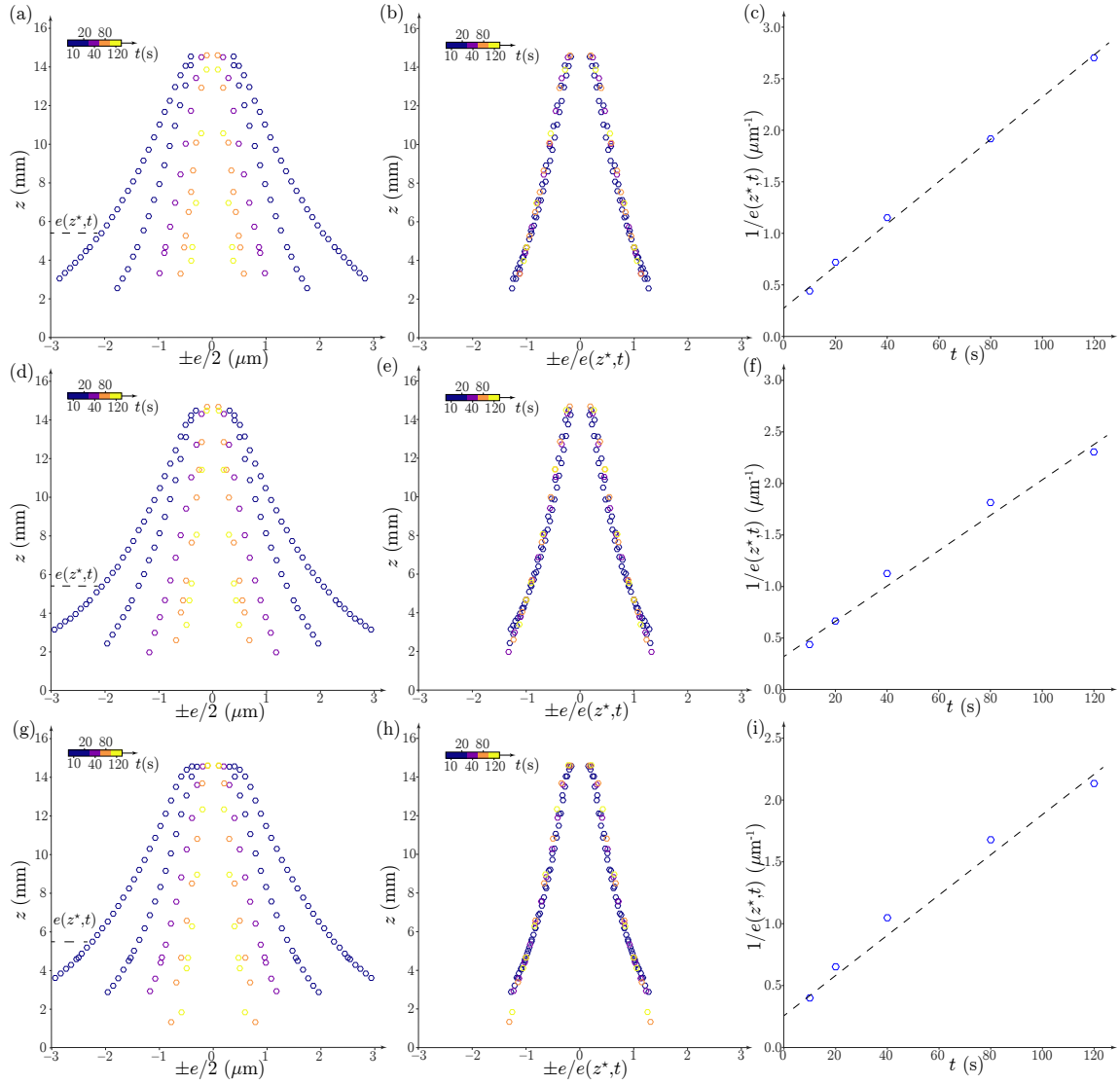


FIG. 8. (a) Thickness profiles at different times, coded in colors, adapted from Fig. 7 (a) in Yu *et al.* [35]. (b) Rescaled profiles obtained after normalizing by $e(z^*, t)$. (c) $1/e(z^*, t)$ as a function of t to validate the linear relationship between these two quantities. (d-e-f) show the same results from Yu *et al.* as (a-b-c) but for Fig. 7 (b) in Yu *et al.* [35]. (g-h-i) show the same results from Yu *et al.* as (a-b-c) but for Fig. 7 (c) in Yu *et al.* [35].

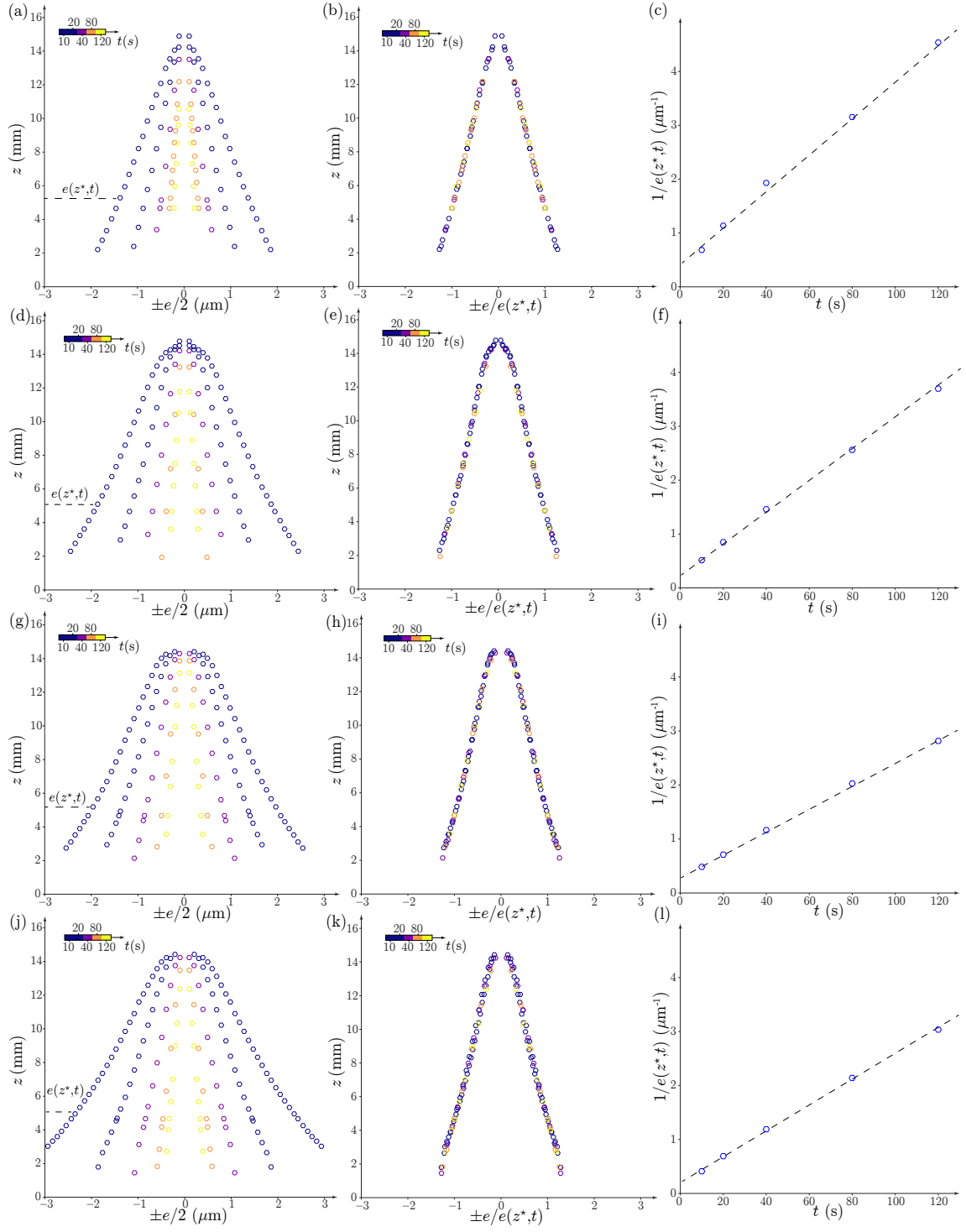


FIG. 9. (a) Thickness profiles at different times, coded in colors, adapted from Fig. 6 (a) in Yu *et al.* [35]. (b) Rescaled profiles obtained after normalizing by $e(z^*, t)$. (c) $1/e(z^*, t)$ as a function of t to validate the linear relationship between these two quantities. (d-e-f) show the same results from Yu *et al.* as (a-b-c) but for Fig. 6 (b) in Yu *et al.* [35]. (g-h-i) show the same results from Yu *et al.* as (a-b-c) but for Fig. 6 (c) in Yu *et al.* (j-k-l) show the same results from Yu *et al.* as (a-b-c) but for Fig. 6 (d) in Yu *et al.* [35].